© 2016. Published by The Company of Biologists Ltd | Journal of Cell Science (2016) 129, 2719-2725 doi:10.1242/jcs.180109

SHORT REPORT

DDA3 and Mdp3 modulate Kif2a recruitment onto the mitotic spindle to control minus-end spindle dynamics

Hye Jin Kwon*, Ji Eun Park*, Haiyu Song and Chang-Young Jang‡

ABSTRACT

Active turnover of spindle microtubules (MTs) for the formation of a bi-orientated spindle, chromosome congression and proper chromosome segregation is regulated by MT depolymerases such as the kinesin-13 family and the plus-end-tracking proteins (+TIPs). However, the control mechanisms underlying the spindle MT dynamics that are responsible for poleward flux at the minus end of MTs are poorly understood. Here, we show that Mdp3 (also known as MAP7D3) forms a complex with DDA3 (also known as PSRC1) and controls spindle dynamics at the minus end of MTs by inhibiting DDA3-mediated Kif2a recruitment to the spindle. Aberrant Kif2a activity at the minus end of spindle MTs in Mdp3-depleted cells decreased spindle stability and resulted in unaligned chromosomes in metaphase, lagging chromosomes in anaphase, and chromosome bridges in telophase and cytokinesis. Although they play opposing roles in minus-end MT dynamics, acting as an MT destabilizer and an MT stabilizer, respectively, DDA3 and Mdp3 did not affect the localization of each other. Thus, the DDA3 complex orchestrates MT dynamics at the MT minus end by fine-tuning the recruitment of Kif2a to regulate minus-end MT dynamics and poleward MT flux at the mitotic spindle.

KEY WORDS: DDA3, Mdp3, Kif2a, Minus-end spindle dynamics, Microtubule flux

INTRODUCTION

Chromosome movement, such as chromosome congression to the mitotic equator and synchronous segregation to opposite sides of the cell during mitosis, is essential for chromosome integrity (Cheeseman and Desai, 2008; Tanaka et al., 2005). The dynamic properties of plus-end microtubules (MTs) are spatially and temporally regulated by different plus-end-tracking proteins (+TIPs), which act primarily as MT-stabilizing factors and link MT ends to cellular structures, such as the cell cortex or kinetochores (Akhmanova and Steinmetz, 2008; Howard and Hyman, 2003; Perez et al., 1999; Schuyler and Pellman, 2001). MT minus-end depolymerization also contributes to MT turnover, whereas MT minus ends in the cell do not grow (Dammermann et al., 2003) because they are capped by specific factors, such as the γ-tubulin ring complex (γ-TURC) (Kollman et al., 2011). α-tubulin–β-tubulin dimers translocate toward the poles through a process termed poleward MT flux, which is based on the depolymerization of the minus ends of spindle MTs at the poles and the net polymerization of their plus ends in the metaphase spindle, resulting in a poleward stream of α-tubulin–β-tubulin (Ganem and Compton, 2006; Kwok and Kapoor, 2007). Thus far, the only known minus end-stabilizing factors are members of the calmodulin-regulated spectrin-associated protein (CAMSAP, also known as patronin) family, which are recruited to growing minus ends to protect them against depolymerizing enzymes (Baines et al., 2009; Goodwin and Vale, 2010; Meng et al., 2008).

Recently, DDA3 (also known as PSRC1) was identified as a new class of spindle dynamics regulator that acts as a MT-destabilizing protein by interacting with the minus-end MT depolymerase Kif2a and the plus-end MT depolymerase MCAK (also known as Kif2C) (Jang and Fang, 2011; Jang et al., 2008). Whereas recombinant DDA3 protein and unphosphorylated DDA3 stabilize MTs in interphase, exhibiting both MT-polymerizing and -bundling activities (Hsieh et al., 2012; Jang et al., 2011), it destabilizes spindle MTs during mitosis by recruiting Kif2a (Jang et al., 2008). Given that DDA3 is hyper-phosphorylated by mitotic kinases, such as Cdk1 and Aurora A during mitosis (Jang et al., 2010, 2011), the function of DDA3 might be converted from an MT stabilizer into an MT destabilizer by phosphorylation at mitotic entry. In addition, DDA3 regulates astral spindle formation and spindle positioning by targeting Cep290 to the centrosome (Song et al., 2015). To understand the detailed regulation mechanism of minus-end spindle dynamics by DDA3, we investigated additional components of the DDA3 complex, with a focus on the MT minus ends. Our results revealed that microtubule-associated protein 7 domain-containing 3 (Mdp3; also known as MAP7D3) forms a mitotic complex with DDA3 and regulates mitotic processes through (1) the inhibition of DDA3-mediated Kif2a recruitment and, concomitantly, (2) fine tuning the turnover of spindle MTs and poleward flux.

RESULTS AND DISCUSSION

Mdp3 forms the DDA3 complex during mitosis

To investigate the molecular mechanism of DDA3-mediated regulation of spindle dynamics, we have previously purified the DDA3 complex from mitotic cells expressing DDA3 C-terminally tagged with the S-peptide and GFP (DDA3–S–GFP), and components of the DDA3 complex were analyzed by mass spectrometry (Jang et al., 2008). Interestingly, Mdp3 was identified as a DDA3-associated protein (Fig. S1A). Although Mdp3 has been identified as a spindle-associated protein through proteomic analysis (Sauer et al., 2005; Sun et al., 2011), its mitotic function has not been characterized. Hence, we asked whether endogenous Mdp3 and DDA3 form a complex during the cell cycle. As expected, DDA3 was detected in the Mdp3 immunoprecipitates in early mitosis but not in interphase (Fig. 1A). Reciprocal immunoprecipitations also showed that DDA3 and Mdp3 co-precipitated in early mitosis (Fig. 1B). Gel filtration analysis of mitotic cell extracts demonstrated the presence of

Research Center for Cell Fate Control, College of Pharmacy, Sookmyung Women's University, Seoul 140-742, Republic of Korea.
*H.J.K. and J.E.P. contributed equally to this work

‡Author for correspondence (cyjang@sookmyung.ac.kr)

C.-Y.J., 0000-0003-3465-5075

Received 9 September 2015; Accepted 25 May 2016

Journal of Cell Science

Journal of Cell Science (2016) 129, 2719-2725 doi:10.1242/jcs.180109

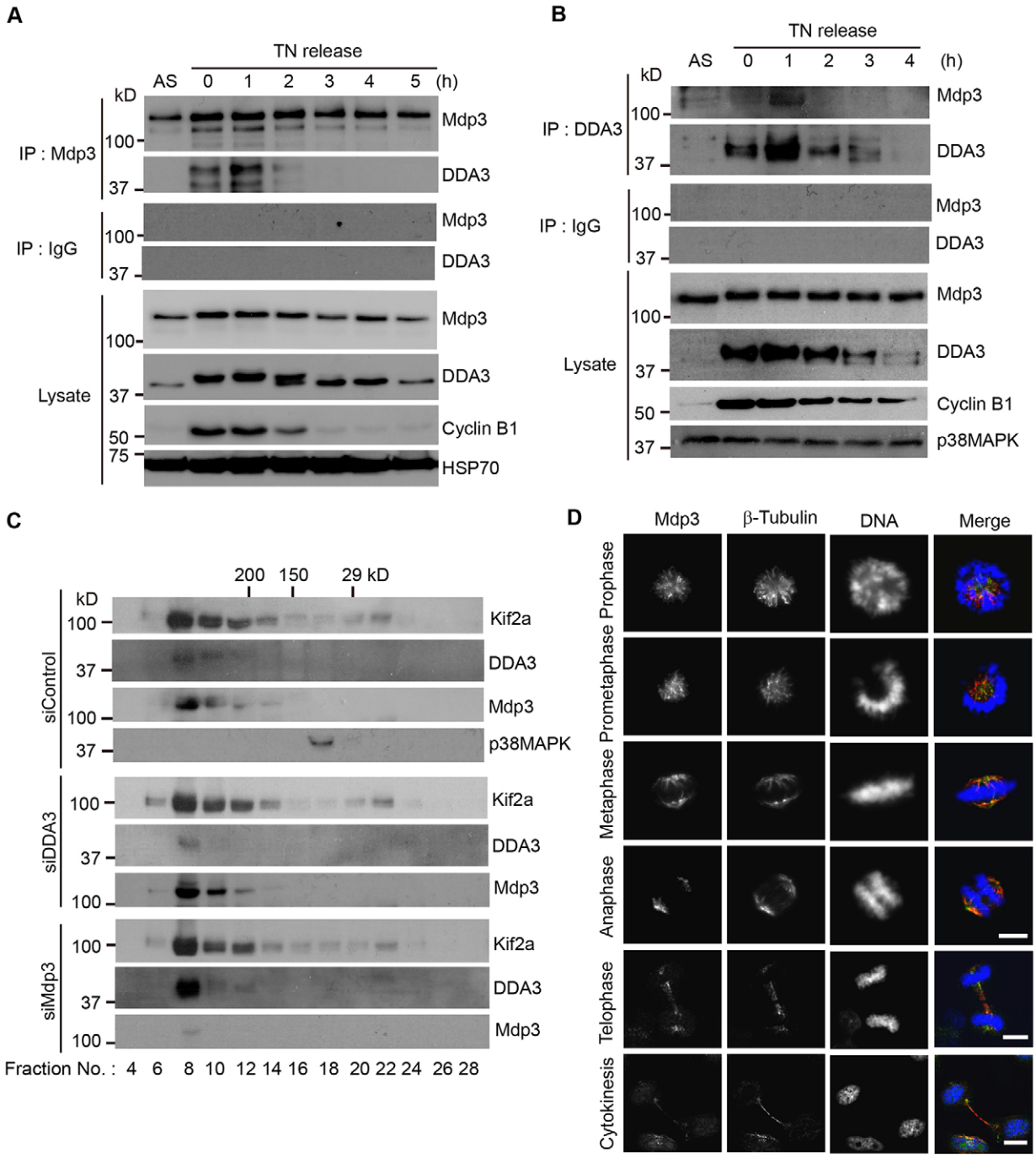

Fig. 1. Mdp3 interacts with DDA3 on the mitotic spindle. (A,B) HeLa S3 cells were synchronized at prometaphase by a thymidine-nocodazole (TN) block, released into fresh medium and harvested at the indicated times. The anti-Mdp3 or anti-DDA3 immunoprecipitations (IP) were analyzed by western blotting. HSP70 and p38 MAPK served as a loading controls. AS, asynchronous cells. (C) At 1 h after release from thymidine-nocodazole block, HeLa S3 cells treated with the indicated siRNA were harvested and cell lysates were separated using a Yarra SEC-3000 column. The indicated fractions were analyzed by western blotting. p38 MAPK served as a loading control. (D) HeLa cells were fixed with methanol and stained for Mdp3 (green), β-tubulin (red) and DNA (DAPI, blue). Scale bars: 5 µm.

Mdp3 and DDA3, as well as Kif2a, in the same molecular mass fractions (Fig. 1C). Strikingly, depletion of DDA3 or Mdp3 increased the level of Mdp3 or DDA3 in the complex, respectively. In agreement with previous findings (Sun et al., 2011), endogenous Mdp3 was localized to the mitotic spindle from prometaphase to anaphase (Fig. 1D) and colocalized with DDA3 at the spindle during metaphase (Fig. S1B). These data indicate that Mdp3 is a new component of the DDA3 complex during mitosis.

Mdp3 is involved in mitotic progression and chromosome movement

To determine the function of Mdp3 in the DDA3 complex, we depleted endogenous Mdp3 protein by using small interfering RNAs (siRNAs) and found a twofold increase in the mitotic index as measured by flow cytometry (Fig. 2A,B). Immunostaining of Mdp3-depleted cells revealed that the loss of Mdp3 localization to the spindle resulted in abnormal spindle structure and chromosome

Journal of Cell Science (2016) 129, 2719-2725 doi:10.1242/jcs.180109

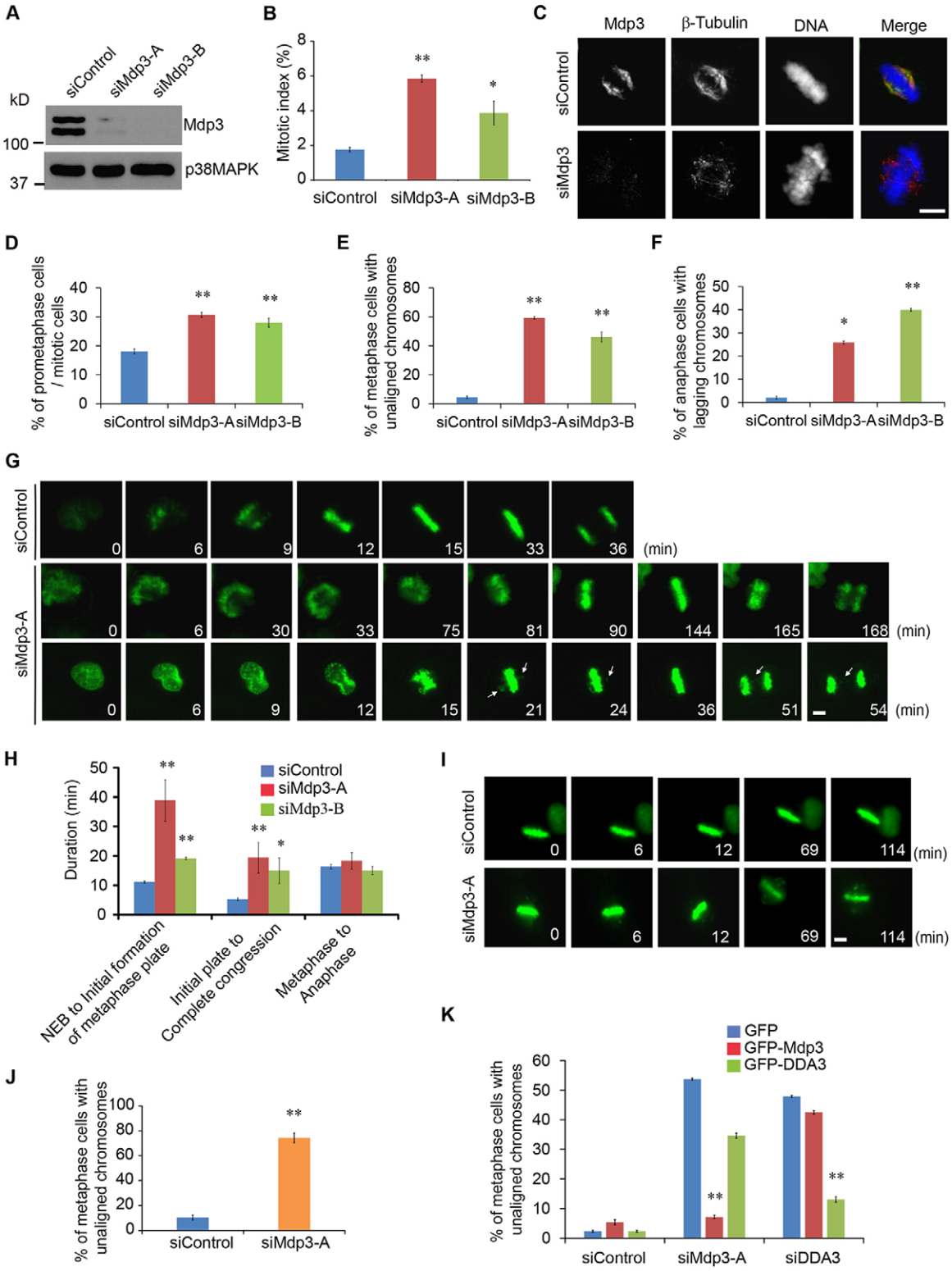

Fig. 2. Mdp3 depletion results in aberrant chromosome alignment and mitotic progression defects. (A,B) At 48 h after transfection, the mitotic index was determined by anti-phospho-MPM2 antibody staining and FACS analysis (B) from three independent experiments. (C–F) The percentage of prometaphase cells (D), metaphase cells with unaligned chromosomes (E), and anaphase cells with lagging chromosomes (after normalization to mitotic cells) (F) were quantified and plotted (n=300 cells). C shows representative images. DNA was stained with DAPI. (G,H) At 48 h after transfection, HeLa cells stably expressing GFP–histone-H2B were filmed for 5 h. The arrows indicate a lagging chromosome in anaphase and a chromosome bridge in telophase and cytokinesis. The duration of mitotic progression was determined (H; n=150 cells). (I,J) At 48 h after transfection, the cells were treated with MG132 and filmed for 5 h. The number of metaphase cells with unaligned chromosomes was plotted (J; n=90 cells). (K) At 48 h after siRNA transfection, the cells were transfected with GFP, GFP–Mdp3 or GFP–DDA3 plasmid. At 28 h after plasmid transfection, the percentages of metaphase cells with unaligned chromosomes normalized to the total number of metaphase cells in GFP-positive cells were quantified and plotted (n=300 cells). Scale bars: 5 µm. Quantitative results are mean±s.e.m. *P<0.05; **P<0.01 (two-tailed Student's t-test).

congression defects in metaphase cells (Fig. 2C). In mitotic cells, we observed a 10% increase in prometaphase cells and more than a tenfold increase in metaphase cells with unaligned chromosomes upon depletion of Mdp3 (Fig. 2D,E). Further analysis revealed a sixfold increase in anaphase cells with lagging chromosomes compared with control cells (Fig. 2F). Consistent with these data, quantitative analysis of mitotic progression by time-lapse imaging indicated that the depletion of Mdp3 prolonged the duration of prometaphase [from nuclear envelope breakdown (NEB) to the initial formation of the metaphase plate] and metaphase (from the initial formation of the metaphase plate to anaphase onset; Fig. 2G, H and Movies 1–3). Remarkably, Mdp3-depleted cells also showed chromosome segregation defects, such as lagging chromosomes in anaphase and chromosome bridges in telophase and cytokinesis (Fig. 2G; Movie 3). To investigate whether Mdp3 is involved in chromosome congression, we sought to arrest cells at metaphase by adding the proteasome inhibitor MG132. Notably, most of metaphase cells depleted of Mdp3 showed severe chromosome congression defects (Fig. 2I,J). Whereas re-expression of GFP–DDA3 or GFP–Mdp3 rescued the mitotic defects caused by depletion of the endogenous proteins, GFP–DDA3 expression in Mdp3-depleted cells or GFP–Mdp3 expression in DDA3-depleted-cells was insufficient to overcome chromosome alignment defects (Fig. 2K; Fig. S1C). Furthermore, the exogenous expression of DDA3 and Mdp3 had no reciprocal effect on their respective localizations (Fig. S1C). These results suggest that Mdp3 and DDA3 play different roles in the same complex with respect to chromosome congression.

Mdp3 is involved in spindle MT attachment and spindle dynamics

To delineate the role of Mdp3 in the DDA3 complex, we asked whether the chromosome congression defect caused by depletion of Mdp3 results from impaired spindle dynamics, as occurs in DDA3-depleted cells. The lack of congression of unaligned chromosomes in Mdp3-depleted cells resulted from the absence of MT attachment, as evidenced by Mad2 and BubR1 remaining on the kinetochores of unaligned chromosomes (Fig. 3A,B). However, the depletion of Mdp3 did not abolish the tension across sister kinetochores of aligned chromosomes (Fig. 3C) and decreased the interpolar distance (Fig. 3D), suggesting that depletion of Mdp3 increases spindle dynamics in addition to disruption of spindle attachment. Consistent with this, spindle MT immunofluorescence intensity decreased by 50% in Mdp3-depleted cells compared with control cells (Fig. 3E). As expected, the spindle MT fluorescence intensity significantly increased (by 100%) in cells overexpressing Myc–Mdp3 compared with control cells (Fig. 3F,G). We consistently found that spindle MTs in Mdp3-depleted cells were more sensitive to limited nocodazole treatment and repolymerized more slowly than in control cells (Fig. 3H,I), indicating that Mdp3 is involved in spindle MT polymerization and/or stabilization.

Mdp3 counteracts DDA3 in minus-end MT dynamics

As DDA3 regulates spindle dynamics by recruiting Kif2a, and depletion of Mdp3 destabilizes spindle MTs, we reasoned that the decrease in spindle stability and consequent chromosome alignment defects in Mdp3-depleted cells could be explained by an overloading of Kif2a onto the spindle. To explore this idea further, we confirmed the interaction between Mdp3 and Kif2a during mitosis by immunoprecipitation using an anti-Mdp3 antibody (Fig. 4A). Consistent with the results shown in Fig. 1C, depletion of DDA3 or Mdp3 increased the interaction between Mdp3 and Kif2a, or DDA3 and Kif2a (Fig. 4B,C), respectively. As a result, the level of Kif2a on the spindle (Fig. 4D,E) and around the spindle pole increased upon Mdp3 depletion (Fig. 4F). Furthermore, Kif2a recruitment was diminished in cells overexpressing Myc–Mdp3 compared with control cells (Fig. 4G–I). Because the levels of spindle MTs and Kif2a in DDA3 and Mdp3 double-depleted cells were similar to those in DDA3-depleted cells (Fig. 4J,K; Fig. S2A,B), we conclude that Mdp3 acts as a negative regulator against DDA3 for Kif2a recruitment. Although the increase in tubulin levels in DDA3-depleted cells impaired chromosome alignment (Jang et al., 2008), chromosome congression was not perturbed by the increase in tubulin levels in Mdp3-overexpressing cells (Fig. 2K). Because, in the same manner, the decrease in tubulin levels in DDA3-overexpressing cells also did not disrupt chromosome congression (Fig. 2K), we reasoned that endogenous DDA3 in Mdp3-overexpressing cells or Mdp3 in DDA3-overexpressing cells might compensate for overexpression effects of Mdp3 or DDA3 on chromosome congression, respectively. To analyze the effect of Mdp3 on spindle dynamics, the turnover rates of α-tubulin–β-tubulin heterodimers on the mitotic spindle were measured using a fluorescence loss in photobleaching (FLIP) experiment. In contrast to cells in which DDA3 was depleted (Jang et al., 2008), the half-life of GFP–α-tubulin was decreased in Mdp3-depleted cells (Fig. S2C–E; Movies 4 and 5). To analyze the effect of Mdp3 and DDA3 on minus-end MT dynamics, the recovery rate of GFP signals in the bleached region was measured using a fluorescence recovery after photobleaching (FRAP) experiment. Although depletion of Mdp3 increased the recovery rate by facilitating MT flux, DDA3 depletion decreased the recovery rate compare to control cells (Fig. 4L; Fig. S3A, Movies 6–8). To measure the velocity of poleward flux directly, the region of interest (ROI) in the spindle was bleached continuously while time-lapse images were captured every 1 s to record the expansion of bleached region. As expected, depletion of Mdp3 increased the speed of poleward flux (Fig. 4M; Fig. S3B, Movies 9–11), suggesting that Mdp3 negatively regulates minus-end MT dynamics and MT flux by inhibiting Kif2a recruitment.

MT minus ends are clustered at a high density in the globular centrosomal regions and are capped with γ-TURC, and for this reason, the molecular machinery of spindle dynamics at the minus end remains relatively uncharacterized compared with the plus end (Kollman et al., 2011). The data presented here suggest a new regulatory mechanism for MT minus-end dynamics by demonstrating that the DDA3 complex modulates the level of Kif2a at the minus end of MTs to orchestrate minus-end MT dynamics and poleward MT flux. In future studies, it will be important to investigate the molecular linker for the cross-talk between plus- and minus-end MT dynamics. Elucidation of the physiological function and the regulatory circuit of DDA3 complex in mitosis will open the door to investigate its role and regulatory mechanism in chromosome integrity and tumor development.

MATERIALS AND METHODS

Plasmids and antibodies

The full-length Mdp3 gene was purchased from OriGene (UAS) and subcloned into the pCS2+ vector with an N-terminal GFP or Myc tag.

The following antibodies were used for western blotting: anti-HSP70 (SC-66048, Santa Cruz Biotechnology; 1:10,000), anti-p38-MAPK (SC-535, Santa Cruz Biotechnology; 1:2000), anti-Mdp3 (HPA035598, Sigma; 1:1000), anti-cyclin B1 (SC-594, Santa Cruz Biotechnology; 1:2000), anti-Myc (SC-789, Santa Cruz; 1:2000), and anti-Kif2a (NB500-180, Novus Biologicals; 1:2000).

Journal of Cell Science (2016) 129, 2719-2725 doi:10.1242/jcs.180109

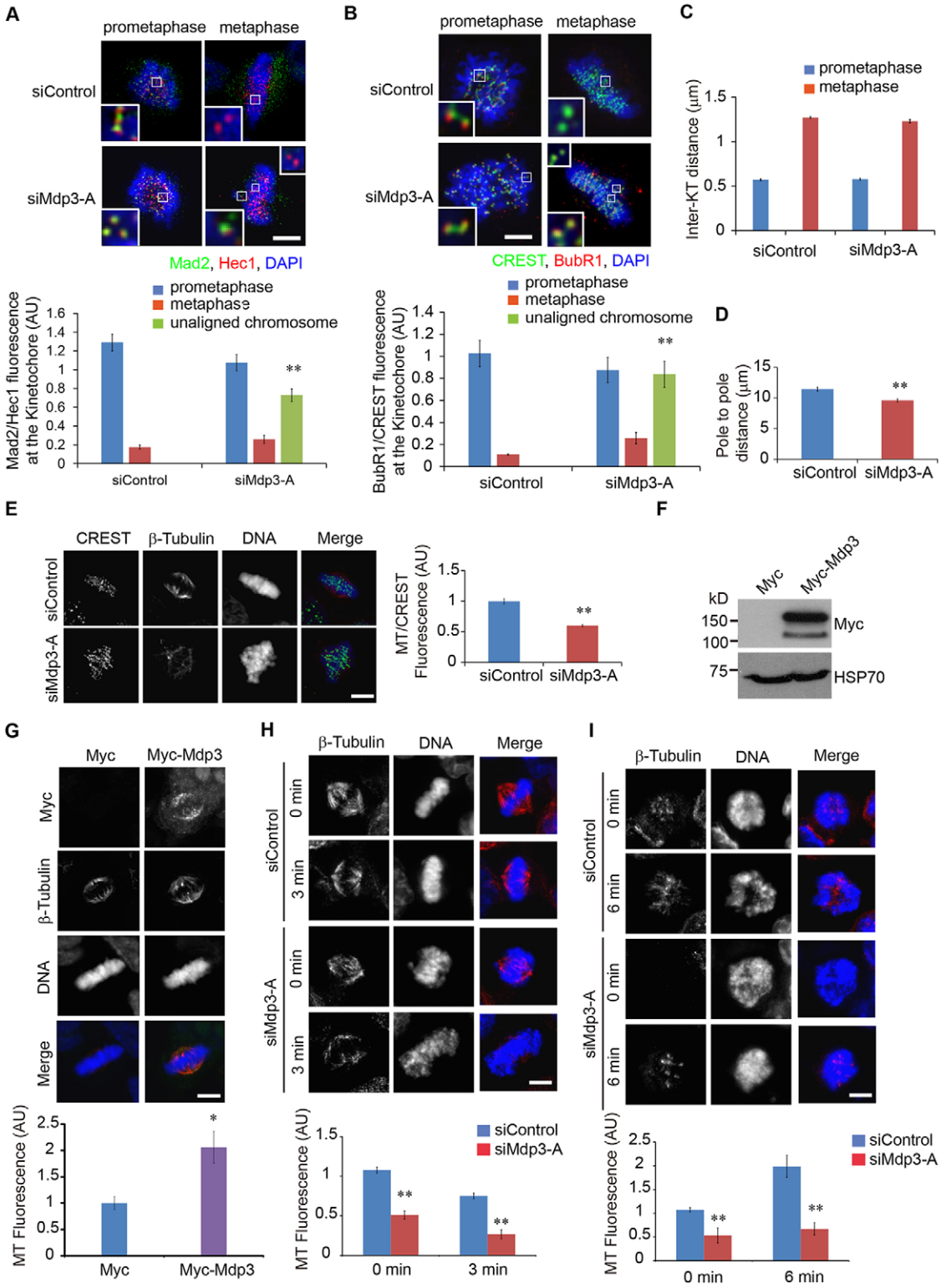

Fig. 3. Mdp3 is involved in spindle MT–kinetochore attachment and spindle MT polymerization. (A,B) Mad2 (A) and BubR1 (B) signals at the kinetochores are shown for cells treated with the indicated siRNA. Insets show single focal planes of the boxed regions. The signal intensity was quantified and normalized to the Hec1 or CREST intensity of the same kinetochores (*n*=300 kinetochores). (C) The distance between sister kinetochores was quantified (*n*=300 kinetochore pairs). (D) Control or Mdp3-depleted cells were stained for γ-tubulin. The distance between centrosome was quantified (*n*=30 cells). (E) Control or Mdp3-depleted cells were stained for β-tubulin. The signal intensity was quantified and normalized to the CREST intensity and plotted (*n*=30 cells). (F,G) At 28 h after transfection with Myc or Myc–Mdp3 cells were stained for β-tubulin and imaged. The signal intensity was quantified and plotted (*n*=30 cells). (H) Control and Mdp3-depleted cells were treated with 1 μg/ml nocodazole for 3 min and then analyzed by immunofluorescence for β-tubulin (*n*=30 cells). (I) Control and Mdp3-depleted cells were treated with 1 μg/ml nocodazole for 10 min at 37°C, washed, released into fresh medium, fixed with MeOH at the 6-min time point, and analyzed by immunofluorescence for β-tubulin (*n*=30 cells). Scale bars: 5 μm. AU, arbitrary units. Quantitative results are mean±s.e.m. **P*<0.05; ***P*<0.01 (two-tailed Student's *t*-test).

Journal of Cell Science (2016) 129, 2719-2725 doi:10.1242/jcs.180109

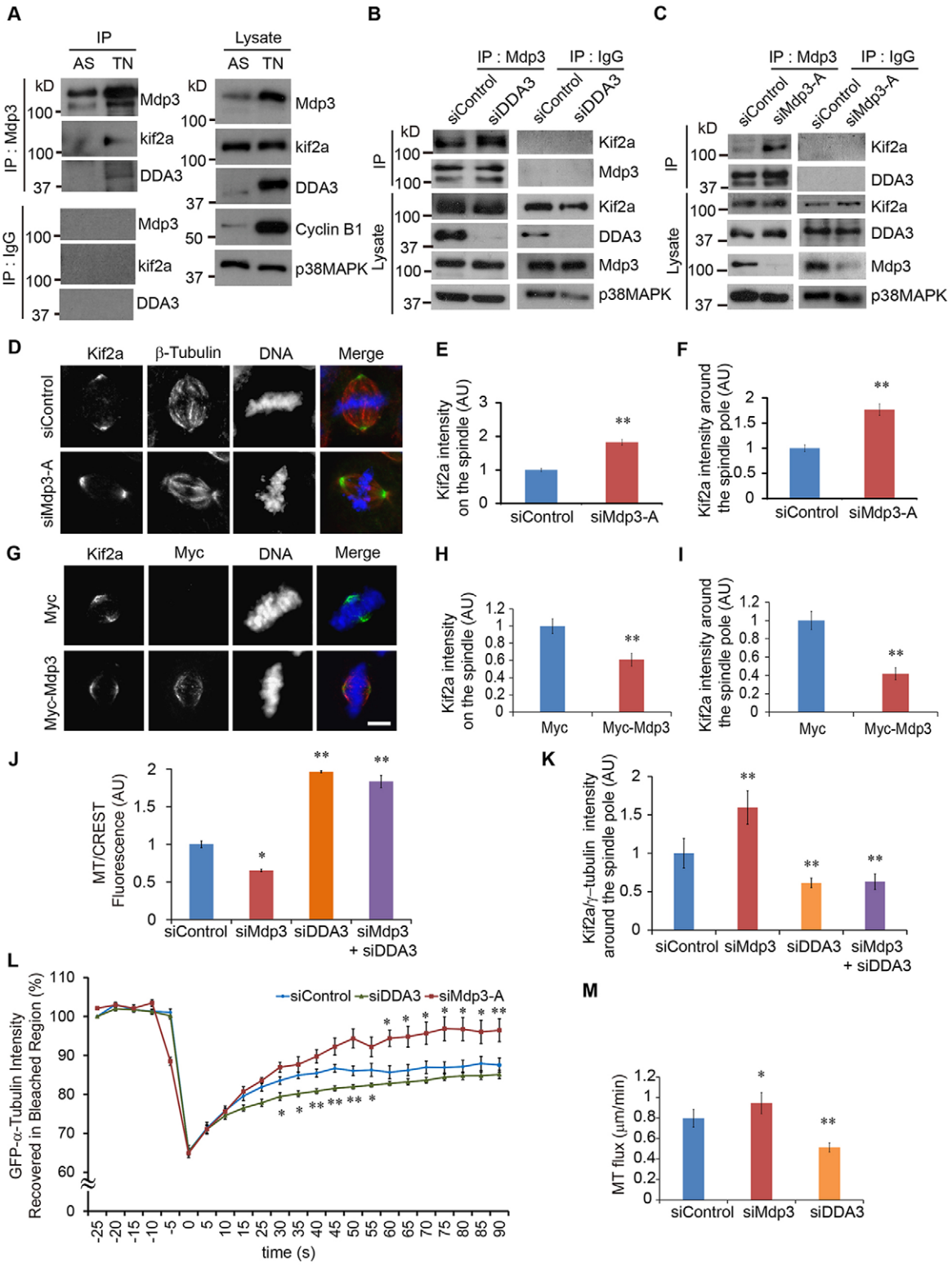

Fig. 4. Mdp3 negatively regulates MT flux by inhibiting DDA3-mediated Kif2a recruitment. (A) HeLa S3 cells were synchronized at prometaphase by a thymidine-nocodazole (TN) block and the anti-Mdp3 immunoprecipitates (IP) were analyzed by western blotting. AS, asynchronous cells. (B,C) At 48 h after transfection with the indicated siRNA, the cells were harvested and the anti-DDA3 or anti-Mdp3 immunoprecipitates were analyzed by western blotting. (D–F) The immunofluorescence intensity for Kif2a in siControl- or siMdp3-transfected cells was imaged (D), and quantified and plotted (E,F, *n*=30 cells). DNA was stained with DAPI. (G–I) At 28 h after transfection with Myc or Myc–Mdp3, the immunofluorescence intensity for Kif2a was imaged (G), and quantified and plotted (H,I; *n*=30 cells). (J,K) At 48 h after transfection, the immunofluorescence intensity for β-tubulin or Kif2a was quantified and plotted after normalizing to CREST or γ-tubulin, respectively (*n*=30 cells). (L,M) HeLa cells stably expressing GFP–α-tubulin were transfected with control, DDA3- or Mdp3-specific siRNAs. After bleaching at the ROI, recovered GFP signals were quantified and plotted (L; *n*=30 cells). During bleaching at the ROI, the velocity of ROI expansion was quantified and plotted (M; *n*=30 cells). AU, arbitrary units. Scale bar: 5 μm. Quantitative results are mean±s.e.m. **P*<0.05; ***P*<0.01 (two-tailed Student's *t*-test).

Cell culture, siRNAs and transfection

HeLa cells were cultured in Dulbecco's modified Eagle's medium (DMEM, WelGENE Inc.) supplemented with 10% fetal bovine serum (FBS, Invitrogen), penicillin (100 units/ml) and 100 µg/ml streptomycin (Invitrogen) and tested for contamination. The siRNA sequences targeting Mdp3 were 5′-CUAC-AUUCGUCUACUGAUA-3′ (siMdp3-A) and 5′-UAUGAAGAGUCUG-GUAAUA-3′ (denoted siMdp3-B) (Thermo Scientific). The sequence targeting DDA3 was 5′-AAGCAAGACTTCAGTAGCATT-3′ (denoted siDDA3) (Thermo Scientific). The control siRNA (siGL2, denoted siControl) was 5′-CGTACGCGGAATACTTCGATT-3′. siRNAs were transfected into cells using DharmaFect 1 (Dharmacon). The DNA transfection was performed using Lipofectamine 2000 (Invitrogen), according to the manufacturer's protocol.

Immunofluorescence

Immunostaining was performed with standard protocols (Jang et al., 2008). Images were obtained using a 1.4 NA plan-Apo 100× oil immersion lens (Carl Zeiss) and deconvolved using AutoDeblur v9.1 and AutoVisualizer v9.1 (AutoQuant Imaging). All of the images are maximum projections from deconvolved *z*-stacks of 0.2-µm thick focal planes. The images for quantification were acquired under a constant exposure in each channel for all cells and measured fluorescence intensity using AutoVisualizer v9.1. Background levels from ROIs outside of the spindle and with no internal reference were subtracted from the results. Primary antibodies used were against Mad2 (PA5-21594, Thermo Scientific Pierce Antibodies; 1:100), BubR1 (LS-C2771, LifeSpanBioSciences; 1:100), CREST (15-235-0001, Antibodies Incorporated; 1:100), Hec1 (GTX70268, Gentex; 1:100), CENP-E (sc-22790, Santa Cruz Biotechnology; 1:100), Mdp3 (HPA035598, Sigma; 1:100), Kif2a (NB500-180, Novus Biologicals; 1:100), and β-tubulin (E7 monoclonal antibody, AB_2315513, Developmental Studies Hybridoma Bank; 1:100).

Live-cell imaging

For time-lapse microscopy, HeLa cells stably expressing GFP–histone-H2B were cultured in Leibovitz's L-15 medium (Invitrogen) supplemented with 10% fetal bovine serum (Invitrogen) and 2 mM L-glutamine (Invitrogen). The images were acquired every 3 min for 5 h with AxioVision 4.8.2 (Carl Zeiss).

For FLIP, FRAP, and MT flux, HeLa cells stably expressing GFP–α-tubulin were placed in a sealed growth chamber heated to 37°C. GFP–α-tubulin in the cytoplasm or in the spindle was photobleached with a laser, and images were acquired with ZEN software (Carl Zeiss) under a LSM 700 confocal microscope (Carl Zeiss) with a 40× lens.

DDA3 proteomics and gel filtration

The DDA3 complex was purified as described previously (Cheeseman et al., 2004; Jang et al., 2008). For gel filtration, the liquid chromatography analysis of mitotic cell extracts was performed with Vision workstation (Applied biosystems) at the Korea Basic Science Institute (Seoul). Sample was separated on a Yarra SEC-3000 (7.8×300 mm, Phenomenex, Torrance).

Statistical analysis

The data were analyzed using Student's *t*-test. A P-value <0.05 (two-tailed) was considered statistically significant.

Competing interests

The authors declare no competing or financial interests.

Author contributions

C.-Y.J. conceived of the project and wrote the manuscript. J.E.P. and H.J.K. performed most of experiments. H.S. analysed some of the quantitative data.

Funding

This work was supported by National Research Foundation of Korea (NRF) grants funded by the Korea government (MSIP) [grant numbers 2011-0030074, NRF-2015M2B2A9032121 and NRF-2015R1A2A2A01005500].

Supplementary information

Supplementary information available online at
http://jcs.biologists.org/lookup/doi/10.1242/jcs.180109.supplemental

References

Akhmanova, A. and Steinmetz, M. O. (2008). Tracking the ends: a dynamic protein network controls the fate of microtubule tips. *Nat. Rev. Mol. Cell Biol.* **9**, 309-322.
Baines, A. J., Bignone, P. A., King, M. D. A., Maggs, A. M., Bennett, P. M., Pinder, J. C. and Phillips, G. W. (2009). The CKK domain (DUF1781) binds microtubules and defines the CAMSAP/ssp4 family of animal proteins. *Mol. Biol. Evol.* **26**, 2005-2014.
Cheeseman, I. M. and Desai, A. (2008). Molecular architecture of the kinetochore–microtubule interface. *Nat. Rev. Mol. Cell Biol.* **9**, 33-46.
Cheeseman, I. M., Niessen, S., Anderson, S., Hyndman, F., Yates, J. R., III, Oegema, K. and Desai, A. (2004). A conserved protein network controls assembly of the outer kinetochore and its ability to sustain tension. *Genes Dev.* **18**, 2255-2268.
Dammermann, A., Desai, A. and Oegema, K. (2003). The minus end in sight. *Curr. Biol.* **13**, R614-R624.
Ganem, N. J. and Compton, D. A. (2006). Functional roles of poleward microtubule flux during mitosis. *Cell Cycle* **5**, 481-485.
Goodwin, S. S. and Vale, R. D. (2010). Patronin regulates the microtubule network by protecting microtubule minus ends. *Cell* **143**, 263-274.
Howard, J. and Hyman, A. A. (2003). Dynamics and mechanics of the microtubule plus end. *Nature* **422**, 753-758.
Hsieh, P.-C., Chiang, M.-L., Chang, J.-C., Yan, Y.-T., Wang, F.-F. and Chou, Y.-C. (2012). DDA3 stabilizes microtubules and suppresses neurite formation. *J. Cell Sci.* **125**, 3402-3411.
Jang, C.-Y. and Fang, G. (2011). DDA3 associates with MCAK and controls chromosome congression. *Biochem. Biophys. Res. Commun.* **407**, 610-614.
Jang, C.-Y., Wong, J., Coppinger, J. A., Seki, A., Yates, J. R., III and Fang, G. (2008). DDA3 recruits microtubule depolymerase Kif2a to spindle poles and controls spindle dynamics and mitotic chromosome movement. *J. Cell Biol.* **181**, 255-267.
Jang, C.-Y., Coppinger, J. A., Yates, J. R., III and Fang, G. (2010). Phospho-regulation of DDA3 function in mitosis. *Biochem. Biophys. Res. Commun.* **393**, 259-263.
Jang, C.-Y., Coppinger, J. A., Yates, J. R., III and Fang, G. (2011). Mitotic kinases regulate MT-polymerizing/MT-bundling activity of DDA3. *Biochem. Biophys. Res. Commun.* **408**, 174-179.
Kollman, J. M., Merdes, A., Mourey, L. and Agard, D. A. (2011). Microtubule nucleation by gamma-tubulin complexes. *Nat. Rev. Mol. Cell Biol.* **12**, 709-721.
Kwok, B. H. and Kapoor, T. M. (2007). Microtubule flux: drivers wanted. *Curr. Opin. Cell Biol.* **19**, 36-42.
Meng, W., Mushika, Y., Ichii, T. and Takeichi, M. (2008). Anchorage of microtubule minus ends to adherens junctions regulates epithelial cell-cell contacts. *Cell* **135**, 948-959.
Perez, F., Diamantopoulos, G. S., Stalder, R. and Kreis, T. E. (1999). CLIP-170 highlights growing microtubule ends in vivo. *Cell* **96**, 517-527.
Sauer, G., Körner, R., Hanisch, A., Ries, A., Nigg, E. A. and Silljé, H. H. W. (2005). Proteome analysis of the human mitotic spindle. *Mol. Cell Proteomics* **4**, 35-43.
Schuyler, S. C. and Pellman, D. (2001). Microtubule "plus-end-tracking proteins": The end is just the beginning. *Cell* **105**, 421-424.
Song, H., Park, J. E. and Jang, C.-Y. (2015). DDA3 targets Cep290 into the centrosome to regulate spindle positioning. *Biochem. Biophys. Res. Commun.* **463**, 88-94.
Sun, X., Shi, X., Liu, M., Li, D., Zhang, L., Liu, X. and Zhou, J. (2011). Mdp3 is a novel microtubule-binding protein that regulates microtubule assembly and stability. *Cell Cycle* **10**, 3929-3937.
Tanaka, K., Mukae, N., Dewar, H., van Breugel, M., James, E. K., Prescott, A. R., Antony, C. and Tanaka, T. U. (2005). Molecular mechanisms of kinetochore capture by spindle microtubules. *Nature* **434**, 987-994.